

Black Hole Shadows in M-theory Scenarios

A. Belhaj^{1*}, M. Benali¹, A. El Balali¹, W. El Hadri¹, H. El Moumni^{2†}, E. Torrente-Lujan^{3‡}

¹ Département de Physique, Equipe des Sciences de la matière et du rayonnement, ESMaR
Faculté des Sciences, Université Mohammed V de Rabat, Rabat, Morocco

² EPTHE, Physics Department, Faculty of Science, Ibn Zohr University, Agadir, Morocco

³ IFT, Dep. de Física, Univ. de Murcia, Campus de Espinardo, E-30100 Murcia, Spain

January 6, 2021

Abstract

We study the shadows of four dimensional black holes in M-theory inspired models. We first inspect the influence of M2-branes on such optical aspects for non-rotating solutions. In particular, we show that the M2-brane number can control the circular shadow size. This geometrical behavior is distorted for rotating solutions exhibiting cardioid shapes in certain moduli space regions. Implementing a rotation parameter, we analyze the geometrical shadow deformations. Among others, we recover the circular behaviors for a large M2-brane number. Investigating the energy emission rate at high energies, we find, in a well-defined approximation, that the associated peak decreases with the M2-brane number. Moreover, we investigate a possible connection with observations (from Event Horizon Telescope or future devices) from a particular M-theory compactification by deriving certain constraints on the M2-brane number in the light of the $M87^*$ observational parameters.

Keywords: Black holes, Shadows, Energy emission rate, M2-branes, M-theory.

*belhadjil@fsr.ac.ma

†hasan.elmoumni@edu.uca.ma

‡torrente@cern.ch

Contents

1	Introduction	2
2	Shadows of non-rotating black holes in M-theory	3
3	Shadows of rotating black holes in M-theory	7
4	Energy emission rate	12
4.1	Non-rotating case	13
4.2	Rotating case	14
5	Observational constraints in the light of the $M87^*$ image	15
6	Discussions and concluding remarks	16

1 Introduction

Black holes were considered, until recently, objects to be treated only by theoretical physics methods. Nowadays, their properties can be also observed, opening new windows in astrophysics, cosmology and the study of gravity at non-trivial regimes. Among others, the physics of such objects has led to remarkable results in many gravity models including M-theory, a candidate for a quantum theory of gravity [1–3].

The first strong indication of the existence of black holes was the observation of the gravitational waves [4]. Later, rather direct, evidence came with the first image of the shadow of the black hole in $M87^*$ galaxy announced by the Event Horizon Telescope (EHT) international collaboration [5, 6]. In the near future, projects like the Black Hole Cam (BHC) envisage to take images for Sagittarius A^* , the supermassive black hole in the center of the Milky Way galaxy [7]. With the $M87^*$ black hole shadow data in hand, we expect to make progress on the understanding of gravity models. The predictions for the black hole physical parameters of any gravity model, General Relativity (GR) and beyond, should be compatible with such observational data, not only at qualitative levels but also at increasing levels of the numerical accuracy.

The EHT data reveals that the $M87^*$ black hole has a mass $M = (6.5 \pm 0.7) \times 10^9 M_\odot$ and a ring of a diameter $\theta_d = 42 \pm 3 \mu as$ [8, 9]. Future improvements of the observations will allow to have more precise and detailed information about the nature of the black hole space-time and strong gravity regimes. Recently, the exploitation of such data has been the object of intensive investigations dealing with the Einstein-Maxwell-Dilaton-Axion, the Einstein-Æther theories of gravity [10, 12], extra dimensions [13] or GR gravity [14]. More details and results on such activities can be found in [15–36].

At low energies, M-theory is usually described by an eleven dimensional supergravity

involving solitonic brane objects. It has been shown that this theory can produce some non-perturbative limits of superstring models after certain compactifications on particular geometries [37]. Up to appropriate approximations, such models have been linked to the black hole physics supported by the AdS/CFT correspondence [3]. In this context, a particular emphasis has been put on the interplay between such a physics on Anti de Sitter (AdS) geometries and thermodynamics. This has opened ways for further research, for example the study of links with black hole thermodynamical aspects. Precisely, phase transitions of numerous AdS black holes have been extensively studied providing non-trivial results [38–41]. More recently, these thermodynamical properties have been combined with optical ones in order to unveil such phase transitions [42]. These optical aspects, concerning the shadow and the deflection angle, have been discussed using different approaches [10, 11]. In particular, it has been revealed that the shadows of non-rotating black holes involve a circular geometry [43]. However, this geometry can be deformed by introducing the spin rotation parameters [44]. It has been reported in multiple studies that the size of such a geometry is sensitive to the physical parameters of beyond-GR models. In particular, it is sensitive to the physical parameters of solutions including dark sectors [45].

The aim of this paper is the investigation of the shadow aspects of four dimensional black holes in M-theory inspired models. We first analyze the M2-brane effect on such optical behaviors for non-rotating solutions. In particular, we show that the M2-brane number can be used to control the circular shadow size. This optical aspect is distorted in rotating solutions involving cardioid shapes for certain moduli space regions. Precisely, we inspect the influence of the M2-brane number and the rotation parameter on the geometrical shadow observables. Moreover, we discuss a possible connection with observations (from Event Horizon Telescope or future devices) associated with a particular M-theory compactification by imposing certain constraints on the M2-brane number in the light of the $M87^*$ observational parameters. Studying the energy emission rate at high energies of such M-theory black holes, we find that the corresponding peak decreases with the M2-brane number among other properties.

The organization of this work is as follows. In section 2, we investigate certain optical aspects of four dimensional non-rotating black holes in M-theory. In section 3, we examine the shadow behaviors of the rotating black holes. The energy emission rate is analyzed in section 4. In section 5, we attempt to give a possible connections with with observations. The last section is devoted to conclusions and open questions.

2 Shadows of non-rotating black holes in M-theory

We focus here on the study of the shadow properties of a non-rotating black hole solution in M-theory with M2-brane objects. The bosonic sector of the corresponding supergravity effective theory at low energies is given by

$$16\pi G_{11} S = \int d^{11}x \sqrt{-h} \left(R - \frac{1}{2} |F_4|^2 \right) - \frac{1}{6} \int A_3 \wedge F_4 \wedge F_4, \quad (2.1)$$

where h is the space-time metric determinant and R represents the scalar curvature. The field strength $F_4 = dA_3$ originates from the gauge potential 3-form A_3 and G_{11} is the eleven dimensional gravitational constant. A close inspection reveals that M-theory involves two brane solutions, the M2 and the M5-branes. The near horizon geometry of such black M-branes can be written as a product of AdS spaces and spheres as follows

$$\mathcal{X}^{M\text{-theory}} = AdS_d \times \mathbb{S}^{11-d}, \quad (2.2)$$

where $d = 4$ or $d = 7$ corresponding to the M2 and the M5-branes respectively [37]. In this work, we will focus on the M2, $d = 4$, case to make contact with observational black hole physics. We expect similar results for the M5-branes since they are dual objects. In particular, we deal with a four dimensional solution relying on the M2-brane physics associated with the geometry

$$\mathcal{X}^{M2} = AdS_4 \times \mathbb{S}^7. \quad (2.3)$$

We assume first the, non-rotating, metric

$$ds^2 = -f(r)dt^2 + \frac{1}{f(r)}dr^2 + r^2(d\theta^2 + \sin^2\theta d\phi^2) + L_{AdS}^2 d\Omega_7^2, \quad (2.4)$$

where $d\Omega_7^2$ indicates the metric of the seven dimensional real sphere with a radius L_{AdS} . In this solution, the metric function $f(r)$ takes the form

$$f(r) = 1 - \frac{m}{r} + \frac{r^2}{L_{AdS}^2}. \quad (2.5)$$

The integration constant m is related to the black hole mass M by the following relation

$$m = 2G_4 \times M, \quad (2.6)$$

where G_4 is the four dimensional gravitational constant. Since the four dimensional AdS solution is obtained from the compactification of the eleven dimensional theory on the seven dimensional sphere, one can obtain

$$G_4 = \frac{G_{11}}{\text{Vol}(\mathbb{S}^7)}, \quad (2.7)$$

where one has

$$G_{11} = 2^4 \pi^7 \ell_p^9, \quad \text{Vol}(\mathbb{S}^7) = \omega_7 L_{AdS}^7. \quad (2.8)$$

Introducing L_{AdS} , it has been shown that the eleven dimensional space-time

$$\mathcal{X}^{M2} = (AdS_4)_{L_{AdS}/2} \times (\mathbb{S}^7)_{L_{AdS}}, \quad (2.9)$$

described by the metric of Eq.(2.4), can be considered as the near horizon geometry of N coincident M2-branes in an eleven dimensional supergravity limit of M-theory. In this way, the AdS radius L_{AdS} can be related to the M2-brane number N via the usual relation

$$L_{AdS}^9 = 2^{-\frac{3}{2}} \pi^3 N^{\frac{3}{2}} \ell_p^9 \quad (2.10)$$

where ℓ_p is the Planck length. In this framework, the mass parameter m becomes a M2-brane number dependent

$$m(N) = \frac{192 \times 2^{1/6} \pi^{2/3} \ell_p^2 M}{N^{7/6}}. \quad (2.11)$$

In this context, the metric function of Eq.(2.5) takes then the form

$$f(r) = 1 - \frac{192 \times 2^{1/6} \pi^{2/3} \ell_p^2 M}{N^{7/6} r} + \frac{2^{1/3} r^2}{N^{1/3} \pi^{2/3} \ell_p^2}. \quad (2.12)$$

To study the null mass geodesics (“photon” orbits) in this geometry, in the presence of M2-branes, we exploit the Hamilton-Jacobi method based on the Carter factorization mechanism developed in [46]. This method has been extensively used in the rotating solutions. Although not strictly necessary for the non-rotating case, its use will allow one to establish a smooth contact with the rotating case which will be studied later on.

According to [47], the photon equation of motion can be obtained using the Hamilton-Jacobi equation

$$\frac{\partial S}{\partial \tau} + \frac{1}{2} g^{\mu\nu} \frac{\partial S}{\partial x^\mu} \frac{\partial S}{\partial x^\nu} = 0, \quad (2.13)$$

where τ is the affine parameter along the geodesics and where S is the Jacobi action written as

$$S = -Et + L\phi + S_r(r) + S_\theta(\theta). \quad (2.14)$$

E and L are the conserved energy and the conserved angular momentum, respectively. $S_r(r)$ and $S_\theta(\theta)$ are functions of r and θ , respectively, which will be absorbed in certain relevant relations. The geodesic equations, controlling the motion of the photon, can be expressed as

$$\frac{dt}{d\tau} = \frac{E}{f(r)}, \quad (2.15)$$

$$\frac{d\phi}{d\tau} = \frac{L}{r^2 \sin^2 \theta}, \quad (2.16)$$

$$r^2 \frac{d\theta}{d\tau} = \pm \sqrt{\Theta(\theta)}, \quad (2.17)$$

$$r^2 \frac{dr}{d\tau} = \pm \sqrt{\mathcal{R}(r)}. \quad (2.18)$$

The expression $\mathcal{R}(r)$ and $\Theta(\theta)$ are given as a function of the Carter constant \mathcal{K} in the following way

$$\mathcal{R}(r) = E^2 r^4 - r^2 f(r) (\mathcal{K} + L^2), \quad \Theta(\theta) = \mathcal{K} - L^2 \cot^2 \theta. \quad (2.19)$$

To analyze the shadow boundary, the expression of the effective potential for a radial motion will be exploited. Using the relation

$$\left(\frac{dr}{d\tau} \right)^2 + V_{eff}(r) = 0, \quad (2.20)$$

we get the effective potential associated with M-theory backgrounds

$$V_{eff}(r) = \left[1 - \frac{192 \times 2^{1/6} \pi^{2/3} \ell_p^2 M}{N^{7/6} r} + \frac{2^{1/3} r^2}{N^{1/3} \pi^{2/3} \ell_p^2} \right] \frac{(\mathcal{K} + L^2)}{r^2} - E^2. \quad (2.21)$$

The unstable circular orbits can be obtained by maximizing the effective potential

$$V_{eff}|_{r=r_0} = \frac{dV_{eff}}{dr}|_{r=r_0} = 0, \quad \mathcal{R}(r)|_{r=r_0} = \frac{d\mathcal{R}(r)}{dr}|_{r=r_0} = 0, \quad (2.22)$$

where r_0 represents the circular orbit radius of the photon. From the expression of the effective potential, we arrive to the following equations

$$V_{eff}|_{r=r_0} = \frac{dV_{eff}}{dr}|_{r=r_0} = \begin{cases} \left[1 - \frac{192 \pi^{2/3} 2^{1/6} \ell_p^2 M}{N^{7/6} r} + \frac{2^{1/3} r^2}{N^{1/3} \pi^{2/3} \ell_p^2} \right] (\mathcal{K} + L^2) - r^2 E^2 = 0, \\ \left[2r - \frac{576 \pi^{2/3} 2^{1/6} \ell_p^2 M}{N^{7/6}} \right] (\mathcal{K} + L^2) = 0. \end{cases} \quad (2.23)$$

It can be shown that the effective potential of a four dimensional non-rotating black hole involves a maximum for the photon sphere radius r_0 given by

$$r_0 = \frac{288 \times 2^{1/6} \pi^{2/3} \ell_p^2 M}{N^{7/6}}. \quad (2.24)$$

Now we are in position to discuss the shadow shapes in M-theory in the absence of the spin parameter. For that purpose, we define the impact parameters η and ξ by

$$\xi = \frac{L}{E}, \quad \eta = \frac{\mathcal{K}}{E^2}. \quad (2.25)$$

With the help of Eq.(2.23) and Eq.(2.25), we obtain a real algebraic equation in terms of η and ξ

$$\eta + \xi^2 = \frac{248832 \pi^{4/3} 2^{1/3} N^{1/3} \ell_p^4 M^2}{248832 (2\pi)^{2/3} \ell_p^2 M^2 + N^{8/3}}. \quad (2.26)$$

To visualize the shadow of the four dimensional black hole from M-theory, we shall introduce the celestial coordinates α and β reported in [47]. For simplicity reasons, we consider such coordinates in the equatorial plane $\theta = \frac{\pi}{2}$. Using Eq.(2.15) and Eq.(2.16), one obtains

$$\alpha = \lim_{r_O \rightarrow \infty} \left(\frac{r_O p^\phi}{p^t} \right) = -\xi, \quad (2.27)$$

$$\beta = \lim_{r_O \rightarrow \infty} \left(\frac{r_O p^\theta}{p^t} \right) = \pm \sqrt{\eta}, \quad (2.28)$$

where r_O is the distance between the observer and the black hole. In this way, the relation given in Eq.(2.26) becomes

$$\alpha^2 + \beta^2 = \frac{248832 \pi^{4/3} 2^{1/3} N^{1/3} \ell_p^4 M^2}{248832 (2\pi)^{2/3} \ell_p^2 M^2 + N^{8/3}}, \quad (2.29)$$

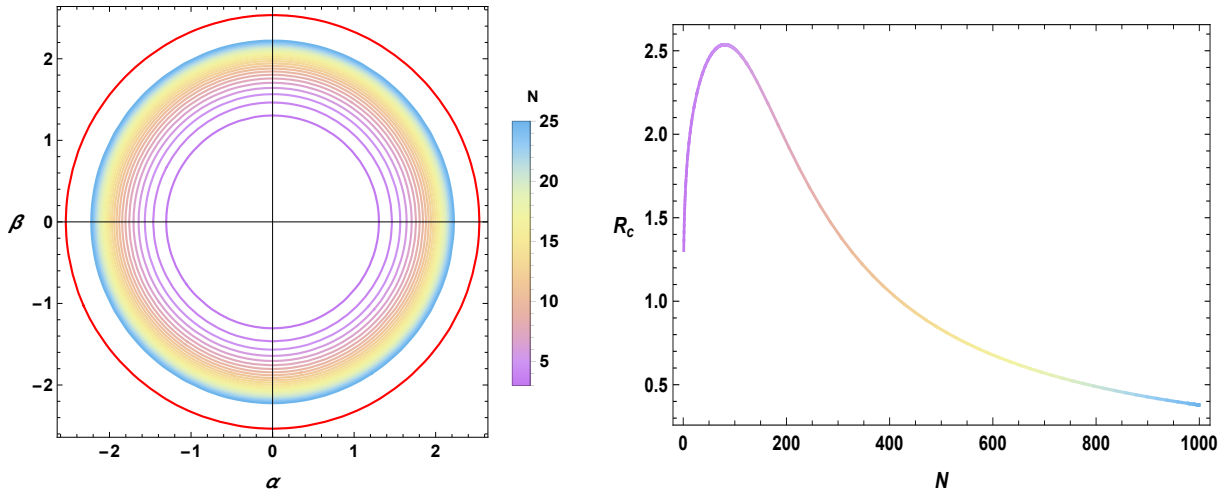


Figure 1: Left: Black hole shadows in the celestial plane ($\alpha - \beta$) for different values of the brane number N , with $\ell_p = 1$ and $M = 1$. The red circle corresponds to $N = 80$. Right: Shadow radius as a function of the brane number.

showing a perfect circular geometry.

To study the M2-brane effect, we inspect the corresponding geometry and the behavior of the shadow radius R_c as a function of N . This is illustrated in Fig.(1).

It follows from this figure that the M2-brane number N , at first, increases the circular size of the black hole shadow reaching a maximal value at

$$N_{max} = 48 \times 7^{-3/8} 3^{7/8} \pi^{1/4} \ell_p^{3/4} M^{3/4} \quad (2.30)$$

giving $N_{max} \approx 80$ for $\ell_p = M = 1$. Then, it decreases towards zero at large values of N ($N \rightarrow \infty$). It is noted that the gap between the circles describing the shadows decreases by increasing the number of M2-branes.

Having discussed the non-rotating case, we consider next the behaviors of rotating M-theory black holes. In particular, we introduce the spinning parameter to deal with the associated optical properties.

3 Shadows of rotating black holes in M-theory

In this section, we study the shadow behaviors of a rotating four dimensional black hole in the presence of N coincident M2-branes. Following [48], the line element, of the corresponding metric solution, reads as

$$ds^2 = -\frac{\Delta_r}{W} \left(dt - \frac{a}{\Xi} \sin^2 \theta d\phi \right)^2 + W \left(\frac{dr^2}{\Delta_r} + \frac{d\theta^2}{\Delta_\theta} \right) + \frac{\Delta_\theta \sin^2 \theta}{W} \left(a dt - \frac{r^2 + a^2}{\Xi} d\phi \right)^2, \quad (3.1)$$

where the involved terms are given by

$$\Delta_r = r^2 - 2mr + a^2 + \frac{r^2}{L_{AdS}^2}(r^2 + a^2), \quad \Delta_\theta = 1 - \frac{a^2}{L_{AdS}^2} \cos^2 \theta, \quad (3.2)$$

$$\Xi = 1 - \frac{a^2}{L_{AdS}^2}, \quad W = r^2 + a^2 \cos^2 \theta. \quad (3.3)$$

To investigate the shadows of such a black hole solution, the equations of motion will be needed. The relevant metric components are

$$g_{tt} = \frac{a^2 \Delta_\theta \sin^2 \theta - \Delta_r}{W}, \quad (3.4)$$

$$g_{t\phi} = g_{\phi t} = \frac{a \sin^2 \theta [\Delta_r - \Delta_\theta (a^2 + r^2)]}{\Xi W}, \quad (3.5)$$

$$g_{\phi\phi} = \frac{\sin^2 \theta [(a^2 + r^2) \Delta_\theta - a^2 \Delta_r \sin^2 \theta]}{\Xi^2 W}. \quad (3.6)$$

Using the equation of the canonical conjugated momentum, we get

$$\dot{t} = \frac{E g_{\phi\phi} + L g_{t\phi}}{(g_{t\phi})^2 - g_{tt} g_{\phi\phi}}. \quad (3.7)$$

Replacing each metric component by its expression, we obtain

$$W \frac{dt}{d\tau} = \frac{(r^2 + a^2) [E (r^2 + a^2) - a L \Xi]}{\Delta_r} + \frac{a (L \Xi - a E \sin^2 \theta)}{\Delta_\theta}. \quad (3.8)$$

The second components of the light rays velocity are given by

$$\dot{\phi} = -\frac{E g_{t\phi} + L g_{tt}}{(g_{t\phi})^2 - g_{tt} g_{\phi\phi}}, \quad (3.9)$$

$$W \frac{d\phi}{d\tau} = \Xi \left[\frac{E a (r^2 + a^2) - a^2 L \Xi}{\Delta_r} + \frac{E a \sin^2 \theta - L \Xi}{\sin^2 \theta \Delta_\theta} \right]. \quad (3.10)$$

The last two components of the velocity light rays can be obtained by considering the Hamilton-Jacobi equation governing the geodesic motion in the space-time. Using the separable variable method developed in [47], we can get the null geodesic equations for the photon particle around a rotating black hole in the presence of N coincident M2-branes. Concretely, they are given by

$$W \frac{dt}{d\tau} = E \left[\frac{(r^2 + a^2) [(r^2 + a^2) - a \xi \Xi]}{\Delta_r} + \frac{a (\xi \Xi - a \sin^2 \theta)}{\Delta_\theta} \right], \quad (3.11)$$

$$W \frac{dr}{d\tau} = \pm \sqrt{\mathcal{R}(r)}, \quad (3.12)$$

$$W \frac{d\theta}{d\tau} = \pm \sqrt{\Theta(\theta)}, \quad (3.13)$$

$$W \frac{d\phi}{d\tau} = E \Xi \left[\frac{a (r^2 + a^2) - a^2 \xi \Xi}{\Delta_r} + \frac{a \sin^2 \theta - \xi \Xi}{\sin^2 \theta \Delta_\theta} \right]. \quad (3.14)$$

In the M-theory rotating case, the expressions of $\mathcal{R}(r)$ and $\Theta(\theta)$ are found to be

$$\mathcal{R}(r) = E^2 \left[[(r^2 + a^2) - a\xi\Xi]^2 - \Delta_r \left[\frac{(a - \xi\Xi)^2}{\Delta_\theta} + \eta \right] \right], \quad (3.15)$$

$$\Theta(\theta) = E^2 \left[\eta\Delta_\theta - \cos^2\theta \left(\frac{\xi^2\Xi^2}{\sin^2\theta} - a^2 \right) \right]. \quad (3.16)$$

As in the non-rotating solution, the unstable circular orbits correspond to the maximum value of the effective potential. Roughly, a generic solution of such impact parameters can be given in terms of r_0 , N , a and θ being needed for making contacts with other results including the observational ones. In fact, they are given by

$$\xi = \frac{(r^2 + a^2) \Delta'_r - 4r\Delta_r}{a \Xi \Delta'_r} \Big|_{r=r_0}, \quad (3.17)$$

$$\eta = \frac{r^2 (16 a^2 \Delta_r \Delta_\theta - (r\Delta'_r - 4\Delta_r)^2)}{a^2 \Delta_r'^2 \Delta_\theta} \Big|_{r=r_0}, \quad (3.18)$$

where one has used $\Delta'_r = \frac{\partial\Delta_r}{\partial r}$. Precisely, an appropriate calculation generates the following relations

$$\xi = \frac{a^2 (\mu - \nu r_0^3 + r_0) + r_0^2 (r_0 - 3\mu) - a^4 \nu r_0}{a (a^2 \nu - 1) (a^2 \nu r_0 - \mu + 2\nu r_0^3 + r_0)}, \quad (3.19)$$

$$\eta = \delta + \frac{4a^4 \nu r_0^2 \cos^2(\theta) (a^2 (\nu r_0^2 + 1) + r_0 (-2\mu + \nu r_0^3 + r_0))}{a^2 (a^2 \nu \cos^2(\theta) - 1) (a^2 \nu r_0 - \mu + 2\nu r_0^3 + r_0)^2} \quad (3.20)$$

where δ , μ , and ν are expressed as follows

$$\delta = \frac{r_0^3 (4a^2 \mu + 6r_0^2 (a^2 \mu \nu + \mu) - r_0^3 (a^2 \nu - 1)^2 - 9\mu^2 r_0)}{a^2 (a^2 \nu \cos^2(\theta) - 1) (a^2 \nu r_0 - \mu + 2\nu r_0^3 + r_0)^2}, \quad (3.21)$$

$$\mu = \frac{192 \times 2^{1/6} \pi^{2/3} \ell_p^2 M}{N^{7/6}}, \quad (3.22)$$

$$\nu = \frac{2^{1/3}}{N^{1/3} \pi^{2/3} \ell_p^2}. \quad (3.23)$$

Now, we analyze the shadow behaviors of a particular situation. Placing an observer at infinity and considering the photons (null mass) near the equatorial plane $\theta = \frac{\pi}{2}$, we obtain the impact parameters

$$\xi = \frac{a^2 (\mu - \nu r_0^3 + r_0) + r_0^2 (r_0 - 3\mu) - a^4 \nu r_0}{a (a^2 \nu - 1) (a^2 \nu r_0 - \mu + 2\nu r_0^3 + r_0)}, \quad (3.24)$$

$$\eta = \frac{r_0^3 (4a^2 \mu + 6r_0^2 (a^2 \mu \nu + \mu) - r_0^3 (a^2 \nu - 1)^2 - 9\mu^2 r_0)}{a^2 (a^2 \nu r_0 - \mu + 2\nu r_0^3 + r_0)^2}. \quad (3.25)$$

Following [47], the celestial coordinates in the equatorial plane given by Eq.(2.27) and Eq.(2.28) are modified in the rotating case as follows

$$\alpha = -\frac{\xi}{\sin\theta_0}, \quad (3.26)$$

$$\beta = \pm \sqrt{\eta + a^2 \cos^2\theta_0 - \xi^2 \cot^2\theta_0}, \quad (3.27)$$

where θ_0 is the inclination angle.

Using the expression of Eqs.(3.24)-(3.25), and the celestial coordinates in the equatorial plane, we can illustrate the shadows of such a four dimensional rotating black hole for certain regions of the moduli space.

In what follows, we discuss the effect of the parameter a on M-theory shadow behaviors. It is worth noting that we recover the circular geometry of the non-rotating case from very small values of a , turning off the geometrical spinning effect. Using the real solutions of Eqs.(3.24)-(3.25), we plot in Fig.(2) the associated shapes for different values of the M2-brane number N and the rotation rate a .

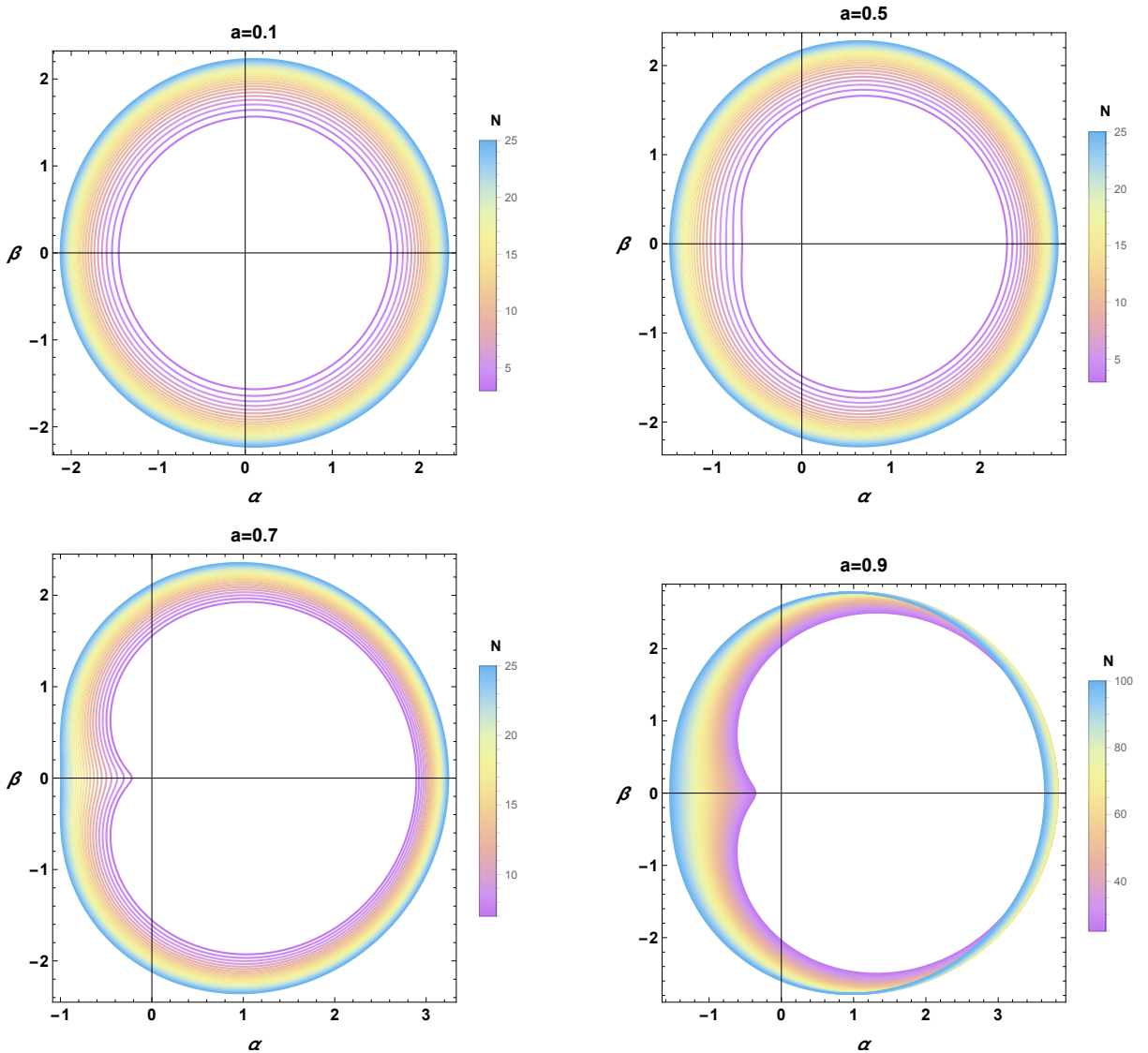


Figure 2: Shadow behaviors of a rotating black hole for different values of M2-brane number N and the rotating rate a , for $\ell_p = 1$ and $M = 1$.

We observe from this figure that for small values of the rotation rate a , the shadows

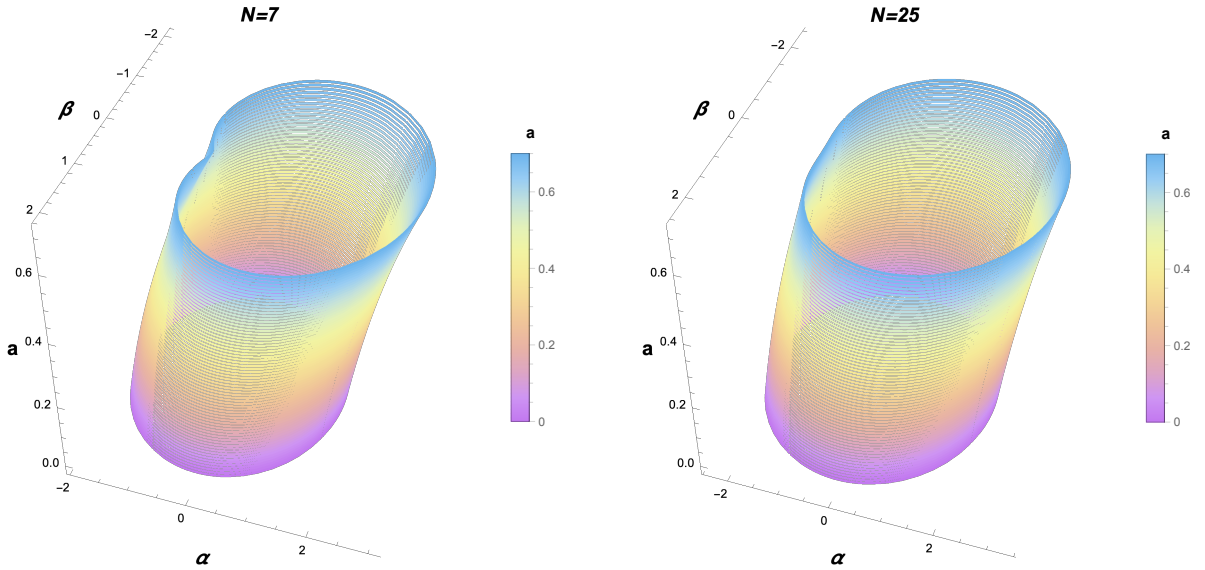


Figure 3: Shadow behaviors inspired by geometric fibrations for $N = 7$ and $N = 25$ with $\ell_p = 1$ and $M = 1$.

maintain the same circular geometries being slightly unsymmetrical about the central axes. In such a region of the moduli space, the M2-brane number plays the same role as in the non-rotating case by controlling the shadow size. Increasing the value of the rotation rate a , the shadows are shifted from the center providing a D-shape. However, such a D-shape changes to a cardioid geometry by decreasing the number N of the M2-branes. This behavior has been obtained from other effects including the stringy and the dark matter sectors [49, 50]. It would be interesting to come back to this remark in future works. It is noted that when we increase the brane number, such a shape becomes circular again showing that the brane number effect can oppose to the rotation one.

It is useful to change the role of a from a parameter to a variable. This will reduce the associated moduli space by considering the M2-brane number as a relevant parameter. In this regard, the shadow geometry will be embedded in a three dimensional space, instead of the two dimensional one. For $N \leq 25$, these geometric configurations are illustrated in Fig.(3). As expected, the M2-brane number is confirmed as a real size parameter of the shadow fiber over the interval $([0, 0.7])$ corresponding to the spinning coordinate. In particular, we remark that the size of the shadow fiber augments over the segment base. Inspecting the M2-brane effect, we realize that two behaviors could appear. For small values of such a parameter, the shadow fiber develops D and cardioid shapes. However, we recover circular fibers by augmenting the M2-brane number. For a very large number of M2-branes, the fiber size starts to decrease until it shrinks to zero.

We approach now the study of observables which can be useful for making contact with other results concerning the rotating black holes. Two astronomical observables R_c and δ_c controlling the size and the shape of the shadows, respectively, will be considered. Following

[44, 51], the size is defined by three specific points which are the top and the bottom position of shadows (α_t, β_t) , (α_b, β_b) and a reference point $(\tilde{\alpha}_p, 0)$. The point of the distorted shadow circle $(\alpha_p, 0)$ meets the horizontal axis at α_p . In this way, the distance between the two latter points is given in terms of a diameter parameter

$$D_c = \tilde{\alpha}_p - \alpha_p = 2R_c - (\alpha_r - \alpha_p). \quad (3.28)$$

In this geometrical picture, the parameter R_c of the shadow is approximatively given by

$$R_c \simeq \frac{(\alpha_t - \alpha_r)^2 + \beta_t^2}{2|\alpha_t - \alpha_r|}. \quad (3.29)$$

The distortion parameter is characterized by the ratio of D_c and R_c

$$\delta_c = \frac{D_c}{R_c}. \quad (3.30)$$

It is straightforward to find analytic expressions for the theoretical predictions of such quantities in terms of microscopical parameters. We plot the results in Fig.(4) where we present R_c and δ_c as a functions of the rotation parameter a and the M2-brane number N . It is observed that, for a fixed rotation rate a , the shadow size increases for large brane number values N . The same behavior appears by fixing N and increasing the spinning parameter a . Besides, the shadow size is larger for $a \simeq 0.99$ in comparison with other values of the parameter a . Moreover, the distortion parameter δ_c , at fixed values of the rotating parameter a , decreases for large values of N . For a fixed brane number N , however, the distortion parameter δ_c increases when the parameter a does. Taking $a = 0.1$, it has been shown that the distortion is almost null providing a circular geometry. A similar behavior is recovered in terms of N . For values bigger than $N = 100$, for instance, the distortion becomes very small implying that one can recover the perfect circular geometry.

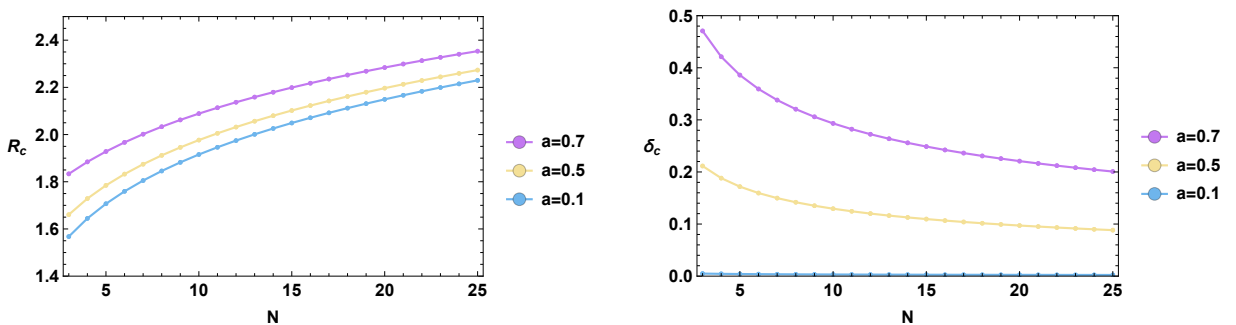


Figure 4: Astronomical observables R_c and δ_c , for different values of N and a with $\ell_p = 1$ and $M = 1$.

4 Energy emission rate

It is recalled that, for a far distant observer and very high energies, the absorption cross-section approaches the geometrical optical limit associated with the shadow of the black

hole. In other regimes, the absorption cross-section oscillates around this geometrical limit. This limit has been expressed in terms of the geodesic properties for various theories. It has been considered as the geometrical cross section of the photon sphere. Based on this approximation, it takes the following form

$$\frac{d^2 E(\omega)}{d\omega dt} = \frac{2\pi^3 R_c^2}{e^{\frac{\omega}{T_i}} - 1} \omega^3, \quad (4.1)$$

where ω is the emission frequency and R_c is the shadow radius [52]. Here, T_i denotes the temperature of the involved black hole given in terms of the horizon radius r_h .

4.1 Non-rotating case

We first consider the non-rotating solution dealt with in the second section. For this solution, the temperature is expressed as

$$T_{nr} = \frac{1}{2\pi r_h} \left(1 - \frac{192 \pi^{2/3} 2^{1/6} \ell_p^2 M}{N^{7/6} r_h} + \frac{2^{4/3} r_h^2}{\pi^{2/3} \ell_p^2 N^{7/6}} \right). \quad (4.2)$$

The energy emission rate is plotted in Fig.(5) as a function of ω for different numbers of M2-branes.

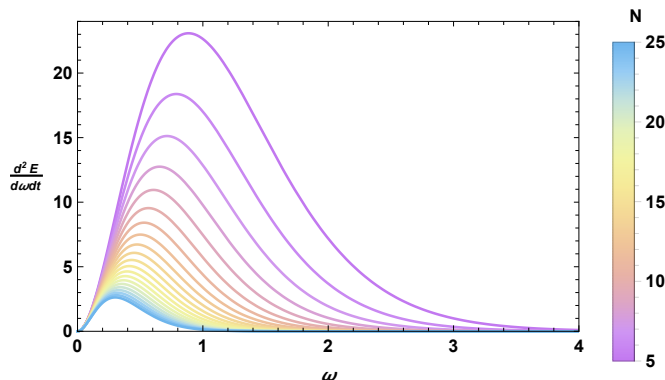


Figure 5: Energy emission rate of non-rotating black holes as a function of the emission frequency for different brane number values, with $\ell_p = 1$ and $M = 1$.

It is remarked from Fig.(5) that, despite the M2-brane number N , the energy emission rate varies slowly. This indicates that the evaporation process for this M-theory black hole can be very slow. Increasing the M2-brane number, we get a lower energy emission rate. This shows that the M2-brane number could be considered as a useful tool to tune the black hole stabilization. For $N \geq 18$, it has been observed that the energy emission rate decreases very slowly. For $N \geq N_{max}$, however, the energy emission rate is almost zero.

4.2 Rotating case

In the rotating case, using similar computations, we should get the temperature expressed in terms of the horizon radius r_h . Indeed, it is found to be given by

$$T_r = \frac{r_h}{2\pi (a^2 + r_h^2)} \left(1 + \frac{2^{1/3} (a^2 + 2r_h^2)}{\pi^{2/3} \ell_p^2 N^{1/3}} - \frac{192 \pi^{2/3} 2^{1/6} \ell_p^2 M}{N^{7/6} r_h} \right). \quad (4.3)$$

As in the previous model case, we illustrate in Fig.(6) the energy emission rate as a function of the emission frequency ω for different numbers of the M2-branes and the rotation rate a .

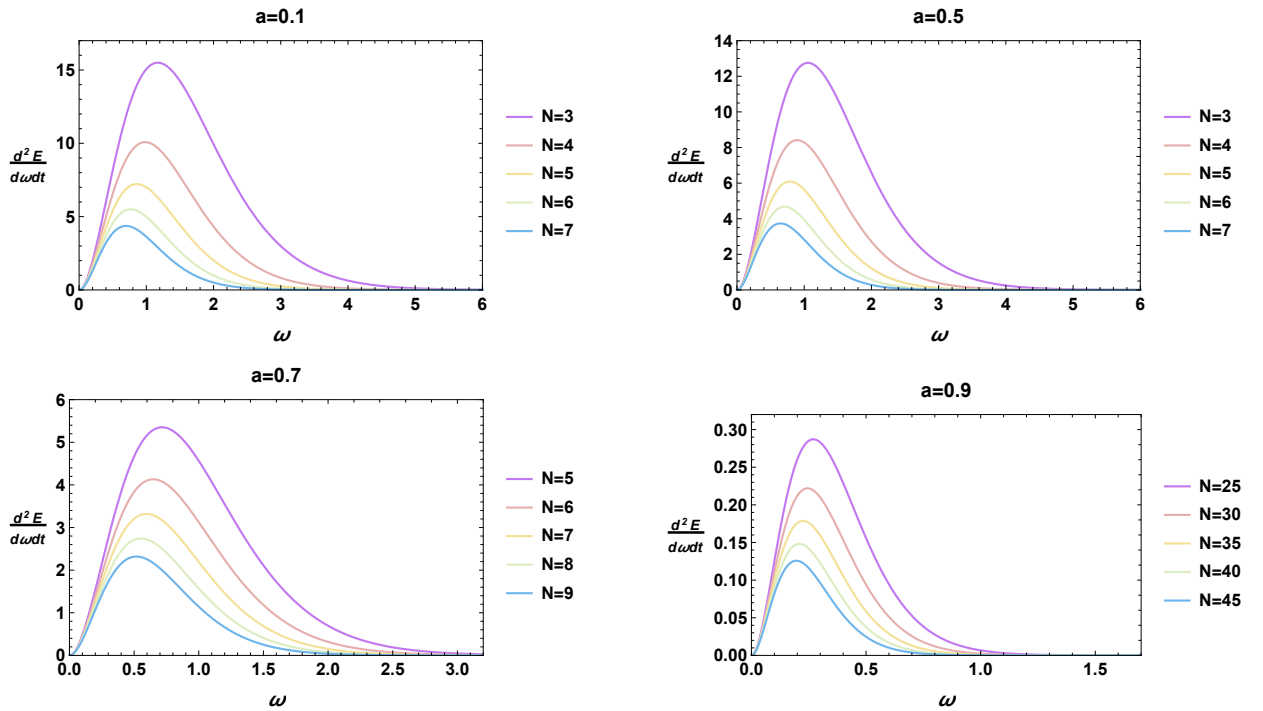


Figure 6: Energy emission rate of rotating black holes as a function of the emission frequency for different values of N and a , with $\ell_p = 1$ and $M = 1$.

We observe, from this figure, a non-trivial behavior in the rotating case. The particle emission rate increases by decreasing the M2-brane number. The evaporation process is clearly faster compared to the non-rotating solution. Increasing the rotation rate parameter, we remark that the emission frequency as well as the energy emission rate are lowered. In this way, we obtain similar effects on the energy emission rate in terms of the M2-brane number as the non-rotating case. Moreover, we find that the energy emission values are quite high compared to the other cases. Increasing the parameter a , one needs more branes to get reasonable results. This can be converted into a constraint on the M2-brane number N provided by the emission rate reality condition, matching with the rotating black hole properties.

5 Observational constraints in the light of the $M87^*$ image

The observation of the shadow of the supermassive black hole $M87^*$, obtained by EHT collaboration, has provided many promoting roads to probe ceratin gravity regimes and alternative physical theories. For such reasons, it should be interesting to make contact with such activities. Indeed, the observational data can put some constraints on the relevant black hole parameters. In this way, the shadow geometrical behaviors can be visualized in terms of the brane number for different values of rotation parameter a . In the unit of $M87^*$ mass, we superpose the shadow of the $M87^*$ black hole modeled by the a Kerr solution (red line) and the shadow of the present M-theory model (cyan line). For different values of a , this behavior is illustrated in Fig7.

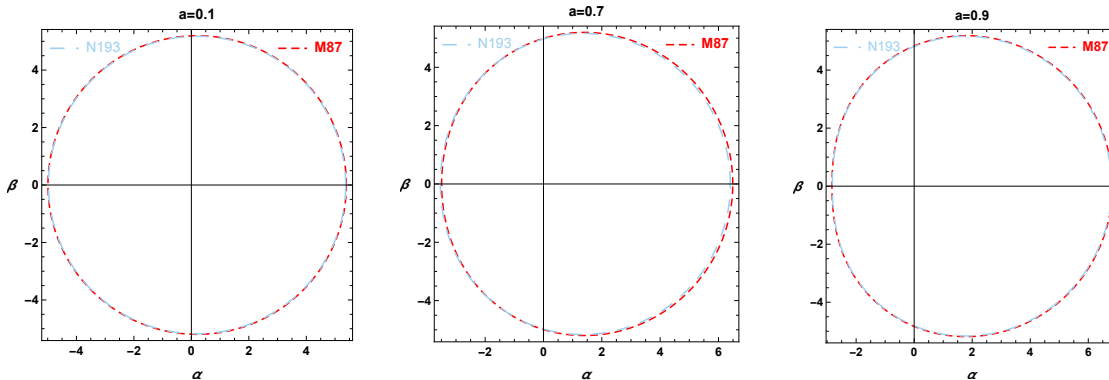


Figure 7: *Black hole shadows for $N = 193$ compared by $M87$ shadow, for different values of a , using $M = 1$ in units of the $M87$ black hole mass given by $M_{BH} = 6.5 \times 10^9 M_{\odot}$ and $r_0 = 91.2kpc$ [49].*

Considering the Fig.(7), a close comparison of the radius of the both black holes reveals that the $M87^*$ shadows could coincide perfectly with the M-theory one for a specific value of the brane number given by $N = 193$. This could constitute an observational constraint on M-theory backgrounds. Knowing that the light of black hole appears distorted, it is crucial to use the distortion parameter to consolidate such a brane number constraint. In Fig.(8), we plot the distortion δ_c of both black holes as a function of the rotating parameter a and the brane number N around the mentioned specific value $N = 193$ (left panel) and the distortion δ_c as a function of a and for $N = 193$ (right panel).

We notice from the left panel of Fig.(8) that the distortion values for $190 < N < 194$ and for $a < 0.6$ is almost null. However, for rotation parameter value $a > 0.6$, the distortion increases by increasing a and N . In the right panel of Fig.(8), we observe that for the specific value of the brane number $N = 193$ and from the value of rotation parameter a , the two distortion values for the black hole in M-theory and $M87^*$ are almost the same. This confirms the specific constraint in the used M-theory backgrounds.

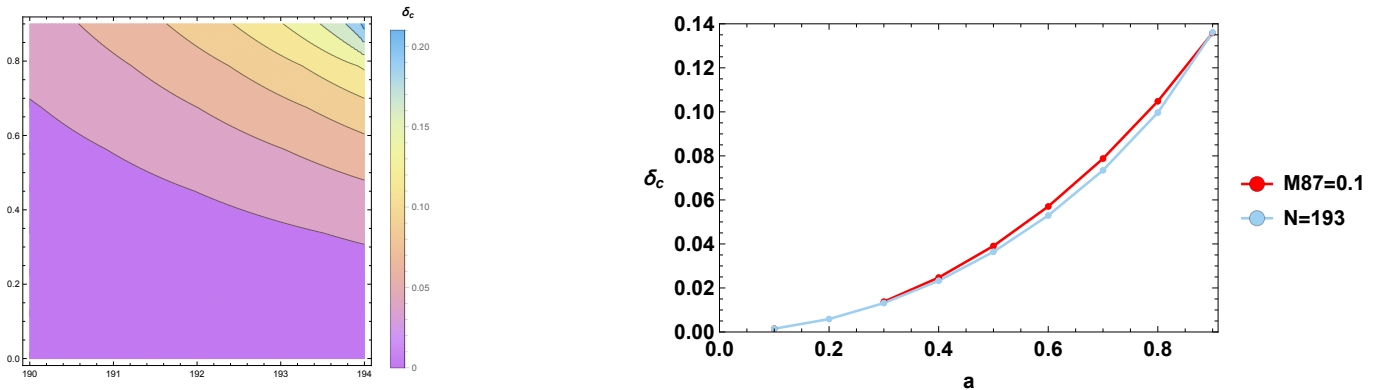


Figure 8: Black hole distortion δ_c for $N = 193$ compared by $M87$ shadow, for different values of a , using $M = 1$ in units of the $M87$ black hole mass given by $M_{BH} = 6.5 \times 10^9 M_\odot$ and $r_0 = 91.2 kpc$.

6 Discussions and concluding remarks

In this work, we have investigated the black hole shadows in M-theory inspired geometries, for both rotating and non-rotating solutions. The present study has been made in terms of a reduced moduli space coordinated by the M2-brane number and the spinning parameter. First, we have considered the photon orbits for non-rotating solutions by establishing the associated shadow circular equations. In particular, we have inspected the effect of the M2-brane number. Such effects have been illustrated for a particular situation relying on the equatorial plane. Concretely, we have realized that the brane physics could be exploited to control the size of such behaviors. As expected, the rotation parameter has been used to distort such a circular black hole shape. In certain regions of the moduli space, we have shown that the shadows change from a D-shape to a cardioid one. A close examination has revealed that this heart shaped could have some relations with the cosmological constant and the charge via brane physics. This observation, being explored and supported by the recent work [50], is the object of further research to be presented elsewhere. In addition, we have promoted the role of the spin quantity from a parameter to a variable. In such a view, the shadows have been viewed as a two dimensional object formed by a one dimensional geometry fibered over the interval describing the rotating spin quantity. In this way, the M2-brane number controls the size of the shadow fibers. Next, we have studied the energy emission rates in certain geometric optical limits. Assuming that the area of the black hole shadow is approximatively the high-energy absorption cross section, we have approached the energy emission rate. The present results have revealed that the M2-brane number effect is the same for the rotating and the non-rotating cases decreasing the energy emission rate. It has been shown that the M2-brane number could be considered as a tuning tool to deal with black hole stabilization issues. For the rotating case, some distinctions appear. Increasing the rotation rate, the emission rate decreases. At the end, using the observational data associated with $M87^*$, we have derived an experimental constraint for which the $M87^*$

shadow can be modeled with a rotating black hole in the M-theory background if the number of the M2-brane is exactly $N = 193$.

This work opens up for further studies. One interesting question is to complete this analysis by considering external sources involving dark sectors associated with axion stringy fields [53]. We hope to report elsewhere on all mentioned open questions.

Acknowledgment

AB would like to thank the Departamento de Física, Universidad de Murcia for very kind hospitality. The authors would like to thank J. J. Fernández-Melgarejo, Y. Hassouni, K. Masmar, M. B. Sedra and A. Segui for discussions on related topics. They are also grateful to the anonymous referee for their careful reading of our manuscript, insightful comments, and suggestions, which have allowed us to improve this paper. The work of ET has been supported in part by the Spanish Ministerio de Universidades and Fundacion Seneca (CARM Murcia) grants FIS2015-3454, PI2019-2356B and the Universidad de Murcia project E024-018. This work is partially supported by the ICTP through AF-13.

References

- [1] I. Bah V. Stylianou, *Gravity duals of $\mathcal{N} = (0, 2)$ SCFTs from M5-branes*, JHEP**04**(2019)050.
- [2] A. Gnechchi, K. Hristov, D. Klemm, C. Toldo, O. Vaughan, *Rotating black holes in 4d gauged supergravity*, JHEP**01**(2014)127.
- [3] J. M. Maldacena, A. Strominger, E. Witten, *Black hole entropy in M theory*, JHEP**12**(1997)002.
- [4] B. Abbott et al., *Observation of Gravitational Waves from a Binary Black Hole Merger*, Phys. Rev. Lett. **116**(6)(2016)061102.
- [5] K. Akiyama et al., *First M87 Event Horizon Telescope Results. I. The Shadow of the Supermassive Black Hole*, Astrophys. J. **L1**(1)(2019)875.
- [6] K. Akiyama et al., *First M87 Event Horizon Telescope Results. IV. Imaging the Central Supermassive Black Hole*, Astrophys. J. **L4**(1)(2019)875.
- [7] C. Goddi et al., *Black Hole Cam: Fundamental physics of the galactic center*, Int.J.Mod.Phys.**D26**02 (2016)1730001.
- [8] K. Akiyama et al., *First M87 Event Horizon Telescope Results. V. Imaging the Central Supermassive Black Hole*, Astrophys. J. **L5**(1)(2019)875.

- [9] K. Akiyama et al., *First M87 Event Horizon Telescope Results. VI. Imaging the Central Supermassive Black Hole*, *Astrophys. J.* **L6**(1)(2019)875.
- [10] S.-W. Wei, Y.-X. Liu, *Observing the shadow of Einstein-Maxwell-Dilaton-Axion black hole*, *JCAP***11**(2013)063.
- [11] A. Belhaj, M. Benali, A. El Balali, H. El Mounni, S-E. Ennadifi, *Deflection Angle and Shadow Behaviors of Quintessential Black Holes in arbitrary Dimensions*, arXiv:2006.01078.
- [12] T. Zhu, Q. Wu, M. Jamil, K. Jusufi, *Shadows and deflection angle of charged and slowly rotating black holes in Einstein-Æther theory*, *Phys. Rev.* **D100**(4)(2019)044055.
- [13] S. Vagnozzin, L. Visinelli, *Hunting for extra dimensions in the shadow of M87**, *Phys. Rev.* **D100**(2)(2019)024020.
- [14] R. Kumar, A. Kumar, S. G. Ghosh, *Testing Rotating Regular Metrics as Candidates for Astrophysical Black Holes*, *Astrophys. J.* **896**(2020)89.
- [15] A. Abdujabbarov, M. Amir, B. Ahmedov, S. G. Ghosh, *Shadow of rotating regular black holes*, *Phys. Rev.* **D93**(10)(2016)104004.
- [16] P.-C. Li, M. Guo, B. Chen, *Shadow of a Spinning Black Hole in an Expanding Universe*, *Phys.Rev.* **D101** (8)(2020)084041, arXiv:2001.04231.
- [17] Z. Stuchlík, D. Zdeněk, C. Daniel, and S. Jan, *Light escape cones in local reference frames of Kerr–de Sitter black hole spacetimes and related black hole shadows*, *Eur. Phys. J. C.* **78**(3)(2018), arXiv:1811.00072.
- [18] C. Bambi, K. Freese, S. Vagnozzi, L. Visinelli, *Testing the rotational nature of the supermassive object M87* from the circularity and size of its first image*, *Phys. Rev.* **D100** (4)(2019)044057.
- [19] P. V. P. Cunha, C. A. R. Herdeiro, E. Radu, H. F. Runarsson, *Shadows of Kerr black holes with scalar hair*, *Phys. Rev. Lett.* **115**(21)(2015)211102.
- [20] E. F. Eiroa, C. M. Sendra, *Shadow cast by rotating braneworld black holes with a cosmological constant*, *Eur. Phys. J.* **C78**(2)(2018)91.
- [21] A. Grenzebach, V. Perlick, C. Lämmerzahl, *Photon Regions and Shadows of Kerr-Newman-NUT Black Holes with a Cosmological Constant*, *Phys. Rev.* **D89**(12)(2014)124004.
- [22] M. Guo, N. A. Obers, H. Yan, *Observational signatures of near-extremal Kerr-like black holes in a modified gravity theory at the Event Horizon Telescope*, *Phys. Rev.* **D98**(8)(2016)084063.

- [23] S. Haroon, M. Jamil, K. Jusufi, K. Lin, R. B. Mann, *Shadow and Deflection Angle of Rotating Black Holes in Perfect Fluid Dark Matter with a Cosmological Constant*, Phys. Rev. **D99**(4)(2019)044015.
- [24] T. Johannsen, A. E. Broderick, P. M. Plewa, S. Chatzopoulos, S. S. Doeleman, F. Eisenhauer, V. L. Fish, R. Genzel, O. Gerhard, M. D. Johnson, *Testing General Relativity with the Shadow Size of Sgr A**, Phys. Rev. Lett. **116**(3)(2016)031101.
- [25] M. Khodadi, A. Allahyari, S. Vagnozzi, D. F. Mota, *Black holes with scalar hair in light of the event horizon telescope*, arXiv:2005.05992.
- [26] A. Övgün, I. Sakalli and J. Saavedra, *Shadow cast and Deflection angle of Kerr-Newman-Kasuya spacetime*, JCAP **10**(2018)041.
- [27] A. Belhaj, A. El Balali, W. El Hadri, M. A. Essebani, M. B. Sedra and A. Segui, *Kerr-AdS Black Hole Behaviors from Dark Energy*, Int. Jour. of Mod. Phys. **D29** (09) (2020) 2050069.
- [28] R. A. Konoplya, T. Pappas, A. Zhidenko, *Einstein-scalar-Gauss-Bonnet black holes: Analytical approximation for the metric and applications to calculations of shadows*, Phys. Rev. **D101**(4)(2020)044054.
- [29] P.-C. Li, M. Guo, B. Chen, *Shadow of a spinning black hole in an expanding universe*, Phy. Rev. **D101**(8)(2020)084041.
- [30] R.-S. Lu, A. E. Broderick, F. Baron, J. D. Monnier, V. L. Fish, S. S. Doeleman, V. Pankratius, *Imaging the Supermassive Black Hole Shadow and Jet Base of M87 with the Event Horizon Telescope*, Astrophys. J. **788**(2014)120.
- [31] T. Ohgami, N. Sakai, *Wormhole shadows in rotating dust*, Phys. Rev. **D94**(6)(2016)064071.
- [32] N. Tsukamoto, *Black hole shadow in an asymptotically-flat, stationary, and axisymmetric spacetime: The Kerr-Newman and rotating regular black holes*, Phys. Rev. **D97**(6)(2018)064021.
- [33] O. Yu. Tsupko, *Analytical calculation of black hole spin using deformation of the shadow*, Phys. Rev. **D95**(10)(2017)104058.
- [34] K. S. Virbhadra, G. F. Ellis, *Schwarzschild black hole lensing*, Phys. Rev. **D62**(8)(2000)084003.
- [35] M. Wang, S. Chen, J. Jing, *Shadows of Bonnor black dihole by chaotic lensing*, Phys. Rev. **D97**(6)(2018)064029.

- [36] Z. Younsi, A. Zhidenko, L. Rezzolla, R. Konoplya, Y. Mizuno, *New method for shadow calculations: Application to parametrized axisymmetric black holes*, Phys. Rev. **D94**(8)(2016)084025.
- [37] E. Witten, *Solutions of four-dimensional field theories via M theory*, Nucl. Phys. **B 500**(1997)3-42.
- [38] A. Belhaj, A. E. Balali, W. E. Hadri, Y. Hassouni, E. Torrente-Lujan, *Phase Transitions of Quintessential AdS Black Holes in M-theory/Superstring Inspired Models*, arXiv:2004.10647.
- [39] A. Belhaj, M. Chabab, H. El Mounni, K. Masmarr, M. Sedra, *On Thermodynamics of AdS Black Holes in M-Theory*, Eur. Phys. J. **C76**(2)(2016)73.
- [40] M. Chabab, H. El Mounni, K. Masmarr, *On thermodynamics of charged AdS black holes in extended phases space via M2-branes background*, Eur. Phys. J. **C76**(6)(2016)304.
- [41] J.-L. Zhang, R.-G. Cai, H. Yu, *Phase transition and thermodynamical geometry of Reissner-Nordström-AdS black holes in extended phase space*, Phys. Rev. **D91**(4)(2015)044028.
- [42] A. Belhaj, L. Chakhchi, H. El Mounni, J. Khalloufi, K. Masmarr, *Thermal Image and Phase Transitions of Charged AdS Black Holes using Shadow Analysis*, arXiv:2005.05893.
- [43] C.-M. Claudel, K. S. Virbhadra, G. F. Ellis, *The geometry of photon surfaces*, Journal of Mathematical Physics **42** (2001)818.
- [44] K. Hioki and K.-I. Maeda, *Measurement of the kerr spin parameter by observation of a compact object's shadow*, Phys. Rev. **D80**(2)(2009)024042.
- [45] R. Konoplya, *Shadow of a black hole surrounded by dark matter*, Phys. Lett. **B795**(2019)1-6.
- [46] B. Carter, *Global structure of the kerr family of gravitational fields*, Phys. Rev. **D174**(5)(1968)1559.
- [47] S. Chandrasekhar, *The mathematical theory of black holes*, Oxford University Press,(69)(1998).
- [48] F. Benini, D. Gang, L. A. P. Zayas, *Rotating black hole entropy from m5-branes*, JHEP **3**(2020)1-40.
- [49] K. Jusufi, M. Jamil, P. Salucci, T. Zhu, S. Haroon, *Black hole surrounded by a dark matter halo in the m87 galactic center and its identification with shadow images*, Phys. Rev. **D100**(4)(2019)044012.

- [50] A. Belhaj, M. Benali, A. El Balali, W. El Hadri, H. El Moumni, *Shadows of Charged and Rotating Black Holes with a Cosmological Constant*, arXiv:2007.09058.
- [51] M. Amir, S. G. Ghosh, *Shapes of rotating nonsingular black hole shadows*, Phys. Rev. **D94**(2)(2016)024054.
- [52] S.-W. Wei, Y.-X. Liu, *Observing the shadow of einstein-maxwell-dilaton-axion black hole*, JCAP**11** (2013) 063.
- [53] B. S. Acharya, S. A. R. Ellis, G. L. Kane, B. D. Nelson, M. Perry, *Categorisation and Detection of Dark Matter Candidates from String/Mtheory Hidden Sectors*, JHEP**09**(2018)130, arXiv:1707.04530.